Modification of the National Weather Service Distributed Hydrologic Model for subsurface water exchanges between grids

Behnaz Khakbaz,[1] Bisher Imam,[1] Soroosh Sorooshian,[1] Victor I. Koren,[2] Zhengtao Cui,[2] Michael B. Smith,[2] and Pedro Restrepo[2]

Received 10 June 2010; revised 28 March 2011; accepted 12 April 2011; published 29 June 2011.

[1] To account for spatial variability of precipitation, as well as basin physiographic properties, the National Weather Service (NWS) has developed a distributed version of its hydrologic component, termed the Hydrology Laboratory-Research Distributed Hydrologic Model (HL-RDHM). Because channels are the only source of water exchange between neighboring computational elements, the absence of such exchange has been identified as a weakness in the model. The primary objective of this paper is to modify the model structure to account for subsurface water exchanges without dramatically altering the conceptual framework of the water balance module. The subsurface exchanges are established by partitioning the slow response components released from the lower layer storages into two parts: the first part involves the grid's conceptual channel, while the second is added to the lower layer storages of the downstream pixel. Realizing the deficiency of the water balance module to locate the lower zone layers in sufficient depths, a complementary study is conducted to test the feasibility of further improvement in the modified model by equally shifting downward the lower zone layers of all pixels over the basin. The Baron Fork at Eldon, Oklahoma, is chosen as the test basin. Ten years of grid-based multisensor precipitation data are used to investigate the effects of the modification, plus shifting the lower zone layers on model performance. The results show that the modified-shifted HL-RDHM can markedly improve the streamflow simulations at the interior point, as well as very high peak-flow simulations at the basin's outlet.

Citation: Khakbaz, B., B. Imam, S. Sorooshian, V. I. Koren, Z. Cui, M. B. Smith, and P. Restrepo (2011), Modification of the National Weather Service Distributed Hydrologic Model for subsurface water exchanges between grids, *Water Resour. Res., 47*, W06524, doi:10.1029/2010WR009626.

1. Introduction

[2] Because surface water and groundwater are interrelated components of a hydrologic system, development of one commonly affects the other. Therefore, understanding the basic principles of interactions between groundwater and surface water (GW–SW), and as such development of the models with coupled GW–SW, has been an active area of research since the 1960s [e.g., *Sophocleous*, 2002; *Tóth*, 1962; *Leavesley et al.*, 1983; *Kim et al.*, 1999; *Beeson et al.*, 2001; *Maxwell and Miller*, 2005; *Croley and He*, 2006; *Kollet and Maxwell*, 2006; *Gulden et al.*, 2007; *Kong et al.*, 2010].

[3] Hydrologic interactions between surface water and groundwater occur vertically by infiltration and exfiltration, as well as horizontally by the subsurface lateral flow through the unsaturated zone [*Sophocleous*, 2002]. The mechanisms by which the subsurface flow reaches the streams of a river network to contribute to the streamflow response of a precipitation event are published in several studies [e.g., *Beven*, 1989; *Dingman*, 1994]. There are also a number of studies in the literature showing the significant role of groundwater in the generation of storm and snowmelt runoff in streams [*Pinder and Jones*, 1969; *Dincer et al.*, 1970; *Freeze*, 1974; *Martinec et al.*, 1974; *Beasley*, 1976; *Sklash and Farvolden*, 1979; *Mosley*, 1979].

[4] Despite the significant contribution of the subsurface flow in stormflow generation, most models still are not well equipped to deal with the multidimensional nature of GW–SW interactions. In the case of distributed watershed models, only considering the vertical interactions of GW–SW results in isolation of the cells in the subsurface, and the cell-to-cell connection is done mostly through surface channel routing. However, there exist some more structurally complex models [e.g., *Leavesley et al.*, 1983; *Beeson et al.*, 2001; *VanderKwaak and Loague*, 2001; *Panday and Huyakorn*, 2004; *Croley and He*, 2006; *Kollet and Maxwell*, 2006; *Qu and Duffy*, 2007] which consider the horizontal interactions of the GW–SW by establishing the subsurface connectivity between their constructing elements [*Van*

[1]Center for Hydrometeorology and Remote Sensing, Department of Civil and Environmental Engineering, University of California, Irvine, California, USA.
[2]Hydrology Laboratory, Office of Hydrologic Development, WOHD-12 NOAA/National Weather Service, Silver Spring, Maryland, USA.

0043-1397/11/2010WR009626

Werkhoven et al., 2008]. The distributed hydrologic model of NWS, which is the Hydrology Laboratory-Research Distributed Hydrologic Model (HL-RDHM) [*Koren et al.*, 2004], falls into the first above mentioned category.

[5] HL-RDHM is a complete and flexible tool for distributed hydrologic modeling research and development, and it serves as a prototype to validate techniques before being operational in NWS offices (HL-RDHM user manual: http://www.cbrfc.noaa.gov/present/rdhm/RDHM_User_Manual.pdf). HL-RDHM has been used in several studies and operational applications [*Moreda et al.*, 2006; *Reed et al.*, 2007]. There have also been a number of studies related to model identification, evaluation, and parameter estimation of the HL-RDHM [e.g., *Yilmaz et al.*, 2008; *Tang et al.*, 2007; *Van Werkhoven et al.*, 2008; *Wagener et al.*, 2009; *Pokhrel et al.*, 2008]. *Reed et al.* [2004] summarized the results of the Distributed Modeling Intercomparison Project (DMIP). They reported that HL-RDHM was one of the best among other participating distributed models, and it exhibited significant improvement in terms of overall and peak flow simulations in all test basins. Because channels are the only source of lateral water exchange between neighboring computational elements in the HL-RDHM, the absence of such an exchange between soil moisture states in adjacent grids has been identified as a weakness in the model [*Koren et al.*, 2004].

[6] The purpose of this study is to introduce an approach to modify the NWS distributed hydrologic model (HL-RDHM) structure to account for subsurface lateral flow without dramatically altering the conceptual framework of the well-studied water balance module. In the following section, a detailed description of the proposed methodology to modify the HL-RDHM structure for subsurface water exchange between grids is presented, followed by a discussion of simulation and results, and finally summary and concluding remarks.

2. Brief Description of the HL-RDHM

[7] HL-RDHM can be utilized in lumped, semidistributed, and fully distributed modes. The model structure is currently defined based on regular rectangular grids represented in the Hydrologic Rainfall Analysis Project (HRAP) projection [*Greene and Hudlow*, 1982]. The HRAP cell is defined at about 4 km $\times$ 4 km resolution. For each constructing element, a water balance model (SAC-SMA [*Burnash et al.*, 1973]) and a hillslope and channel routing component are used to simulate rainfall-runoff processes. Parameters of the HL-RDHM include parameters of the water balance and routing components, which are assumed to be constant within a cell but can be variable over a basin. A priori SAC-SMA parameters developed by *Koren et al.* [2000] are used to account for spatial variability over a basin. Scale factors obtained from calibration of the model can adjust these parameter values. In terms of hillslope routing, three parameters are defined: drainage density, hillslope slope, and roughness. There are two channel routing parameters, which relate the channel discharge to its cross section. Either the Chezy-Manning approximation or rating curve methods can be used to define the channel routing parameters. The model can output streamflow, soil moisture, and evapotranspiration at each grid cell. Readers interested in more details about the HL-RDHM are referred to *Koren et al.* [2004].

3. Modification to the HL-RDHM

[8] One of the key points in developing a coupled surface-subsurface modeling system is the boundary condition at the surface-subsurface interface. *Furman* [2008] defined four different levels of coupling: degenerated uncoupled, externally coupled, iterative coupling, and full coupling. As is the case for most operational watershed models, the HL-RDHM employs the most basic coupling scheme, which is the degenerated uncoupled. In this coupling approach the subsurface flow process is represented by a simple algebraic formulation, which relies on the solution of the surface system. The HL-RDHM mimics the subsurface system into a percolation formulation to interact with the surface component. The water balance component (i.e., the SAC-SMA) adjusts subsurface system states and generates supplementary and primary groundwater flows (slow response components) and three fast response components (i.e., direct runoff, surface runoff, and interflow). In the current structure of the HL-RDHM, the fast response components are routed over the cell's hillslope, while groundwater components bypass the hillslope routing and directly enter into the conceptual channel within the same grid cell. No explicit routing scheme of the subsurface flow is considered in the model's structure. The resulting flow from hillslope routing, along with the slow flow components and outflow from the upstream cell, are routed over the conceptual channel in each grid cell. The basin drainage network, which is the surface flow direction defined by using the basin's Digital Elevation Model (DEM) is transformed to an upstream-to-downstream computational order of grid cells called the flow-connectivity file. Using the flow-connectivity file, a cell-to-cell channel routing carries water to the basin's outlet.

[9] In the proposed modification of the HL-RDHM, it is assumed that the hydraulic gradient of subsurface flow is equal to the ground-surface slope [*Beven and Kirkby*, 1979]. Therefore the same surface flow direction can be utilized as the subsurface flow direction.

[10] Moreover, from the four coupling approaches defined by *Furman* [2008], theoretically the higher the level of coupling, the higher the accuracy should be. However, *Furman* [2008] commented, "it is not yet clear if the coupled formulation is beneficial in terms of accuracy and computational effort." Keeping this in mind, the original SAC-SMA model's coupling approach (i.e., degenerated uncoupled) is selected for the modified version as well. The base flow generated by the water balance component at each grid cell is divided into two parts: one which appears in the conceptual channel within the cell, and the other which is added directly to the percolated water to the lower zone of the subsequent downstream cell on the flow-connectivity network. This formulation is similar to the approach of *Croley and He* [2006]. The biggest uncertainty with the application of this approach comes from the estimation of base flow split fractions. *Croley and He* [2006] introduced empirical parameters to be calibrated without clear physical reasoning. In this study the SAC-SMA, which is the water balance component of the original HL-RDHM, has been replaced by the modified SAC-SMA model for frozen ground effects (SAC-HT) [*Koren*, 2006] in order to estimate the base flow fractions (i.e., referred to as alpha). The SAC-HT dynamically converts the SAC-SMA conceptual soil

moisture states at each grid cell into soil moisture states at physically defined soil layers. It utilizes a set of physical relationships that relate the SAC-SMA model parameters to soil properties, such as hydraulic conductivity, field capacity, wilting point, and porosity, to convert the water contents of the upper and lower zones into soil moisture contents at a couple of physically based soil layers [*Koren et al.*, 2003, 2008]. The parameters of the SAC-HT are exactly the same as the SAC-SMA model, with the addition of two physically based parameters (i.e., STXT: soil texture of the upper layer, and TBOT: climatological annual air temperature). For each pixel, alpha values are estimated by overlapping the physically based soil profile obtained from SAC-HT and the conceptual channel bed elevation within the cell. However, the conceptual channel bed elevation grid is not readily available and should be generated before being utilized for the modification.

3.1. Conceptual Channel Bed Elevation Estimation

[11] In this study a procedure is developed to estimate the channel bed elevation for each grid cell of a basin's domain. The kinematic routing defines the relationships between discharge (Q) and channel cross section (A), as well as between channel top width (B) and depth (H) for all pixels:

$$Q = Q_s \times A^m, \tag{1}$$

$$B = a \times H^b, \tag{2}$$

where Q_s, m, a, and b are the routing parameters available from HL-RDHM parametric data as grids. Using equations (1) and (2), one can define conceptual channel depth (H) as a function of discharge (Q) at each pixel (i) by

$$H_i = f(Q_i) = \left(\frac{b_i + 1}{a_i}\right)^{\frac{1}{b_i+1}} \times Q_{s,i}^{\frac{-1}{m_i(b_i+1)}} \times Q_i^{\frac{1}{m_i(b_i+1)}}. \tag{3}$$

[12] Assuming that the maximum discharge at each cell ($Q_{\max,i}$) occurs at the maximum conceptual channel depth with the water level matching the ground surface, the channel bed elevation ($Z_{\mathrm{ch},i}$) can be estimated as follows:

$$Z_{\mathrm{ch},i} = Z_{\mathrm{surf},i} - \frac{1}{(b_i + 1)} H_{\max,i}, \tag{4}$$

where $Z_{\mathrm{surf},i}$ is an averaged ground-surface elevation at cell (i), and $H_{\max,i}$ is the maximum channel depth calculated from equation (3), assuming $Q_i = Q_{\max,i}$.

[13] In watershed applications the historical maximum discharge is not usually available at each grid cell. For this research, first the historical maximum discharge at the basin's outlet ($Q_{\mathrm{max,outlet}}$) is obtained from the U.S. Geological Survey (USGS) measurement database. Then, the potential maximum runoff depth ($y_{\max}$), which is assumed uniformly distributed over the basin, is calculated by

$$y_{\max} = \frac{Q_{\mathrm{max,outlet}}}{F_{\mathrm{outlet}}}, \tag{5}$$

where F_{outlet} is the accumulated contributing area above the basin's outlet.

[14] Then the potential maximum discharge ($Q_{\max}$) at each grid cell can be estimated as a product of the potential maximum runoff depth ($y_{\max}$) and the accumulated contributing area (F) above grid cell (i):

$$Q_{\max,i} = y_{\max} \times F_i. \tag{6}$$

3.2. Calculation of Alpha Values

[15] To modify the model structure for grid water exchanges, the base flow generated by the water balance is divided into two parts by introducing a multiplication factor called "alpha," which by definition is the fraction of the generated base flow appearing in the cell's conceptual channel. Obviously "1-alpha" represents the fraction of base flow added to the percolated water of the subsequent downstream grid based on the connectivity order. Multiplication factors are considered for both primary and supplemental SAC-SMA model baseflows (i.e., alpha_sup and alpha_prim). The alpha can vary between 0 and 1 with alpha = 0, meaning 100% subsurface water exchange, and alpha = 1, indicating no subsurface water exchange.

[16] In the modified HL-RDHM, the advanced SAC-SMA model (i.e., SAC-HT) is utilized as the water balance component in order to estimate the alpha values. By default, SAC-HT defines five soil layers to cover a 2 m soil profile. However, using the actual parameter values obtained from model calibration, SAC-HT automatically adjusts the default number of soil layers and their thicknesses [*Koren et al.*, 2008] to preserve the correct volumes of the upper and lower model storages.

[17] Assuming that the channel shape is constant in time and only soil moisture states are time dependent, one can define dynamics of the interface between the channel and groundwater. The exact location of the interface between channel and groundwater flow is not well defined, and it is not "mathematically sharp" [*Furman*, 2008]. To be considered as a sharp boundary condition, free (gravitational) water at each SAC-HT layer is assumed to be allocated at the bottom of the storage (see Figure 1). This assumption allows estimation of the groundwater–channel water interface elevation at each simulation time step. To calculate the alpha values, the lower boundary of the primary layer (Z_{prim}) and the primary water surface elevation (Z_{LZFPC}) are first obtained as follows:

$$\begin{aligned} Z_{\mathrm{prim}} &= Z_{\mathrm{surf}} - (\mathrm{UP} + \mathrm{LOW}), \\ Z_{\mathrm{LZFPC}} &= Z_{\mathrm{prim}} + 0.001 \times \frac{\mathrm{LZFPC}}{(S_{\max} - S_{\mathrm{fld}})}, \end{aligned} \tag{7}$$

where Z_{surf} is the ground-surface elevation, UP and LOW are the upper and lower storage thicknesses, respectively, generated by SAC-HT in meters (m), $S_{\max}$ is the soil porosity, S_{fld} is the field capacity, and LZFPC is the lower zone free primary water content in millimeters (mm).

[18] Assuming that the supplemental layer is directly above the primary layer, and that the lower boundary of the supplemental layer is matched with the primary free water surface, the lower boundary of the supplemental layer (Z_{sup}) and the supplemental water surface elevation (Z_{LZFSC}) are then estimated as follows:

$$\begin{aligned} Z_{\mathrm{sup}} &= Z_{\mathrm{LZFPC}}, \\ Z_{\mathrm{LZFSC}} &= Z_{\mathrm{sup}} + 0.001 \times \frac{\mathrm{LZFSC}}{(S_{\max} - S_{\mathrm{fld}})}, \end{aligned} \tag{8}$$

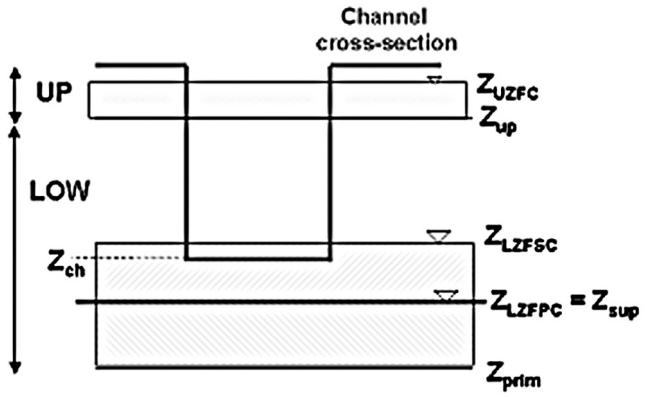

Figure 1. A schematic of the physically based soil profile along with the conceptual channel bed elevation.

where LZFSC is the lower zone free supplemental water content in mm. The alpha_sup and alpha_prim for each pixel are then computed as

$$\text{alpha\_sup} = \frac{(Z_{\text{LZFSC}} - Z_{\text{ch}})}{(Z_{\text{LZFSC}} - Z_{\text{sup}})},$$
$$\text{alpha\_prim} = \frac{(Z_{\text{LZFPC}} - Z_{\text{ch}})}{(Z_{\text{LZFPC}} - Z_{\text{prim}})}. \quad (9)$$

[19] Note that, in some specific cases, equation (9) can yield to alpha_prim (alpha_sup) greater than one. This happens when Z_{prim} (Z_{sup}) is greater than Z_{ch}, such that all of the water in the primary (supplemental) layer appears in the grid's channel. In this case, the numerator in equation (9) becomes greater than the denominator, resulting in an alpha value greater than one. In addition, if the supplemental layer, which by definition is above the primary layer, falls way below the channel bed elevation, the water surface elevations in both primary and supplemental layers become less than the channel bed elevation, which means that no water appears in the cell's channel. Thus, equation (9) leads to negative alpha values. In these particular situations, zero is assigned to any negative alpha values obtained from equation (9), and one is assigned for alphas greater than one.

[20] As one can realize, all variables needed for estimation of the alpha_sup and alpha_prim are calculated from the available information without introducing any new parameters for the modification. In equation (9) the terms Z_{ch}, Z_{prim}, and Z_{sup} are time invariant for each pixel. However, Z_{LZFPC} and Z_{LZFSC} are SAC-SMA model state variables and change over time. Therefore, alpha_prim and alpha_sup are also state variables and need to be calculated for each time step. Figure 1 shows a schematic of the physically based soil profile, along with the conceptual channel bed elevation used herein.

3.3. Advantages and Limitations of the Approach

[21] While watershed models have been improved significantly over the last few decades, a detailed process-based understanding of the hydrologic responses, specifically the surface-groundwater linkage, still eludes the hydrologic community [*Singh and Woolhiser*, 2002]. On the other hand, because of the difficulties and cost of measurement, a detailed, three-dimensional description of the surface microtopography, as well as hydraulic characteristics of soils and underlying geologic materials, cannot be provided [*Woolhiser*, 1996]. Because of these reasons, in real-world applications, watershed models vary in complexity and structure, depending on their purposes. This paper is focused on the improvement of the watershed model applicable to flood predictions at a wide range of river basins. While surface water–groundwater interaction parameterization is developed specifically for the NWS modeling system, it may be applicable to a range of hydrologic models, which do not have explicit channel groundwater interfaces. The introduced modification does not dramatically alter the model's structure, allowing its application with the use of recently available parametric and input data. However, it is flexible in application. If channel characteristics and/or groundwater location are available at the modeling grid resolution, the information can be used instead of a SAC-HT-based procedure to derive the groundwater fractions described in sections 3.1 and 3.2. There is a possibility of simple adjustments to estimated channel bed elevation grid using a basin constant factor considering that the elevation grid preserves spatial variability of the physical properties.

[22] Some limitations need to be considered in specific applications. The parameterization does not have an explicit representation of the subsurface water routing. As such, it can affect intermediate flood shapes and may require manual adjustment to kinematic routing parameters. Mapping conceptual channel storages into a SAC-HT soil profile can lead to considerable uncertainty to derivation of the groundwater-channel bed interface. Some correction/calibration to a priori estimated channel bed elevation might be required.

4. Model Application to the Baron Fork River Basin

[23] The main goals of this application are to: (1) understand the overall performance of the modified HL-RDHM without any parameter calibration using the a priori parameter values and (2) compare the modified model simulations with the original HL-RDHM, when the model parameters are calibrated.

[24] The Baron Fork river basin upstream of the USGS gauging station (07197000) at Eldon, Oklahoma, is chosen as the study basin. This basin, with a drainage area of 795 km^2, is one of the test basins in the Distributed Modeling Intercomparison Project (DMIP) (phases 1 and 2) [*Smith et al.*, 2004] and hereafter is referred to as the Eldon basin. Figure 2 shows the DMIP phase 2 test basins and specified points for the experiment (the Eldon basin is shown with the circle). The industry in the Eldon basin is mainly agriculture, including poultry production and livestock grazing. Elevation changes are mild and range from 214 to 443 m at the highest point in the watershed. The basin's mild topography is evident by the low average slope of 0.5% along its 67 km longest flow path. According to *Smith et al.* [2004], the dominant soil types in the Eldon basin are silty clay (SIC), silty loam (SIL), and silty clay loam (SICL). The average annual rainfall and runoff are 1175 and 340 mm yr^{-1}, respectively. The average annual free water evaporation in the basin is 1089 mm yr^{-1}, with the maximum monthly averages (150 and 157 mm) occurring during the months of June and July, respectively. The Eldon basin has an interior gauge on Baron Fork at Dutch Mills, Arkansas. This interior basin, which occupies 105 km^2, is hereafter called the Dutch basin.

[25] Ten years of hourly NOAA's multisensor (NEXRAD and gauge) data in the HRAP grid format at 4 km × 4 km spatial resolution are used in this study. The 4 km pixel size is used in the model to map this precipitation product. According to *Koren et al.* [2004], this spatial resolution is sufficient for representing the precipitation spatial variability, while maintaining acceptable computational expenses.

[26] A priori parameter grids of the SAC-SMA model developed by *Koren et al.* [2000] at the 4 km scale were made available by NWS over the conterminous United States and used to display the variability of basin properties, which affect runoff-generation processes. Similar resolution grids of hillslope and channel routing parameters were also available for the Eldon basin [*Koren et al.*, 2004; *Reed et al.*, 2002].

Figure 2. The DMIP phase 2 test basins and specified points for the experiment (the Eldon basin is shown with the circle).

4.1. Uncalibrated Experiment

[27] As mentioned earlier, the main goal of this section is to understand the overall performance of the modified HL-RDHM without any parameter calibration using the a priori parameter values. As the first step, the channel bed elevation grid needs to be generated. A subroutine was added to the HL-RDHM to generate this grid automatically, while the remaining parameter grids are ready to be used by the model. The subroutine requires the maximum potential runoff depth (y_{max}) to be entered by the user. Therefore, from the USGS surface water data website (http://waterdata.usgs.gov/usa/nwis/sw), which provides periodic manual measurements of streamflow and gauge height, the historical discharge data measured at the Eldon gauging station are extracted. The discharge values are searched for a "good" rated maximum discharge measurement (here, we chose $Q_{max,outlet}$ = 53,400 cfs (1512 m^3 s^{-1}), which occurred on 21 June 2000). Because the accumulated contributing area above the basin outlet is equal to 795 km^2 (the basin area), the maximum potential runoff depth (y_{max}) that is assumed uniformly distributed over the basin is 1.9 m^3 km^{-2} s^{-1} (i.e., 6.84 mm h^{-1}). The subroutine uses the steps mentioned earlier to generate the channel bed elevation grid and saves the grid to be utilized later in the alpha calculation process. Figure 3 shows the channel bed elevation grid generated for the Eldon basin. It is important to note that the determination of the maximum discharge is a critical stage in the channel bed elevation generation. However, the uncertainty in the measurement of the discharge does not have a significant effect on the overall uncertainty in the generated channel bed elevations. The brief examination of the effect of the errors in the chosen discharge on the generated channel bed elevations showed that 25% assumed error in the measured maximum discharge can change the channel bed elevation estimates by less than 1%. This indicates the negligible sensitivity of the proposed procedure for channel bed elevations to the uncertainty of the measured maximum discharge.

[28] To show where the lower boundaries of the supplemental and primary layers are compared to the channel bed elevation over the test basin, the spatial plots of ($Z_{ch}-Z_{sup}$) (Figure 4a), ($Z_{ch}-Z_{prim}$) (Figure 4b), as well as the river channel network (Figure 4c), are represented for the Eldon basin. These three figures, which are generated using the a priori parameters delivered with the original HL-RDHM, are time invariant. In Figure 4a the two darker pixels

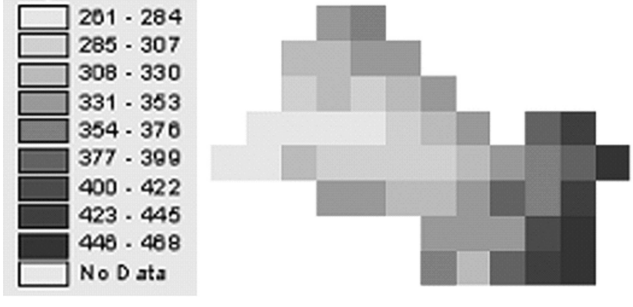

Figure 3. Channel bed elevation grid generated for the Eldon basin.

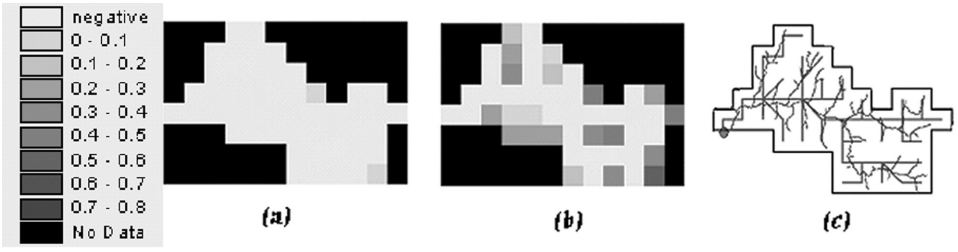

Figure 4. (a) Spatial plots of ($Z_{ch}-Z_{sup}$), (b) ($Z_{ch}-Z_{prim}$), and (c) river channel network for the Eldon basin.

represent the cells where the lower boundary elevations of the supplemental layers are less than the channel bed elevations. Therefore, only these two pixels have the potential to contribute to the supplemental water exchange process. The remaining pixels (which possess negative values) have the lower boundary elevations of supplemental layers greater than the channel bed elevations, and thus pass all of the supplemental water to their channels. Figure 4b shows a greater number of pixels contributing to the primary water exchanges (i.e., cells with darker colors). It is interesting to note that the pixels on the channel network mostly have negative values (i.e., lower boundary elevations of the primary layers greater than the channel bed elevations), and thus do not participate in the primary water exchange process.

[29] The original and modified HL-RDHM models were run for a 10 year period (i.e., 1995–2005) over the Eldon basin using all a priori parameter grids. In this experiment accurate simulations are not expected because a priori parameters do not fully represent the test basin characteristics. However, the runs can provide qualitative information about how the modified model works and to what extent the modification can change the original HL-RDHM simulation results. As an example, Figure 5 shows spatial and temporal variability of alpha_sup and alpha_prim during a storm event over the test basin. For both alpha_sup and alpha_prim plots, the red color represents where the alpha value is equal to 1 (i.e., no contribution to the water exchange process). As expected, the red-color pixels are the same pixels in Figures 4a and 4b that had the lower

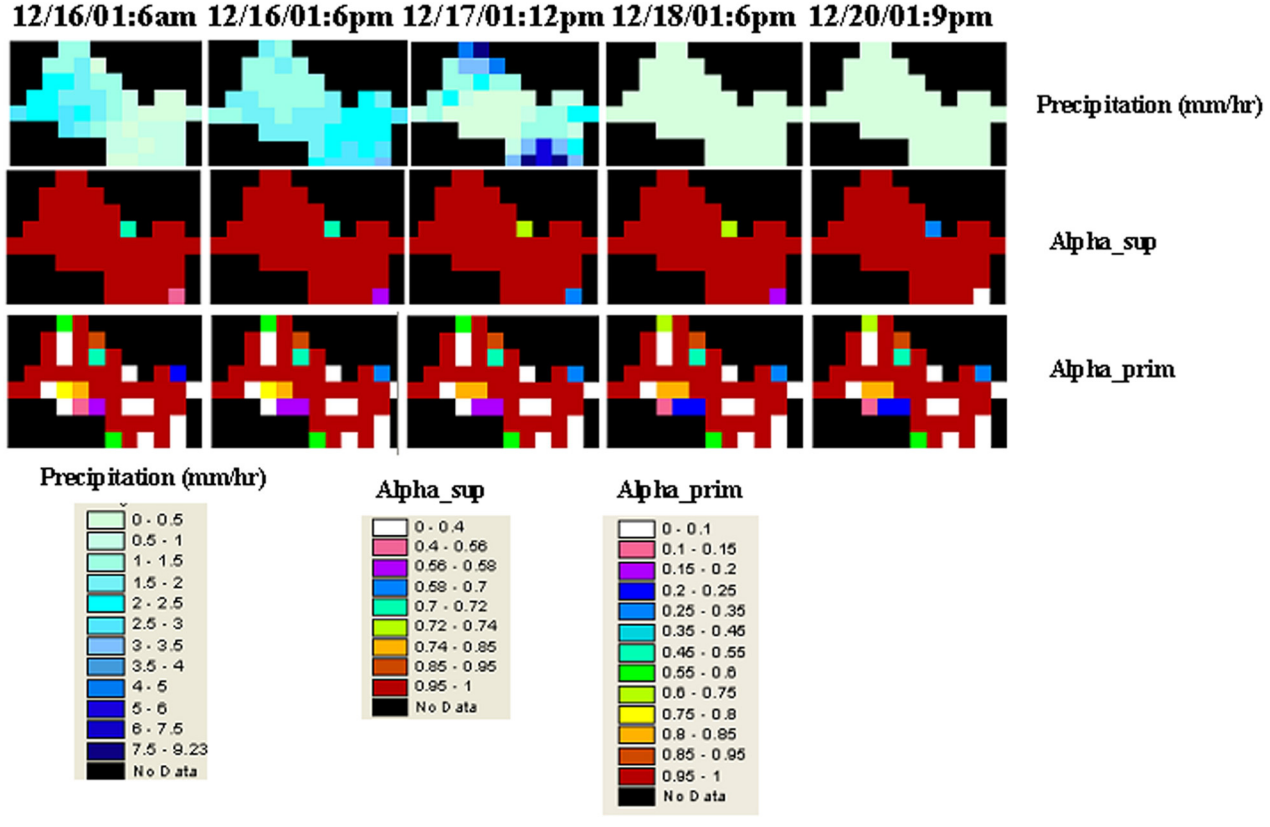

Figure 5. Spatial and temporal variability of alpha_sup and alpha_prim during a storm event over the test basin.

boundary elevations of supplemental/primary layers greater than channel bed elevations. In addition, only the cells that represented the potential to contribute to the water exchanges shown in Figures 4a and 4b possess alpha values less than 1, which in fact agrees with our expectation.

[30] As discussed earlier, and as can be seen in Figures 4 and 5, there are few pixels in the basin that have the potential to contribute to the supplemental water exchange process. In addition, most of the pixels on the channel network do not participate in the primary water exchange process. The main reason for this situation is that SAC-HT, which converts the SAC-SMA model soil moisture states into soil moisture contents, locates the physical layers in a 2 m soil profile. In fact, restriction of the lower zone layers (i.e., related to the groundwater level in real nature) in such a shallow depth could limit participation of several cells over the basin's domain in the subsurface water exchange process. A new methodology to battle this limitation in the modified HL-RDHM model structure will be explored in section 4.1.1.

4.1.1. Shifting the Lower Zone Layers in the Modified HL-RDHM

[31] The modified SAC-SMA model for frozen ground effects (SAC-HT) defines physically based soil layers at relatively shallow depths, which causes alpha values obtained from the modified model to be near or equal to 1 for most of the grids (e.g., in Figure 5), and as such reduces the potential for lateral water exchanges between neighboring cells. In reality, however, groundwater observation records in the Eldon basin show that lower zone layers can be defined at deeper levels. Figure 6 shows the groundwater level records measured at three wells (i.e., wells 9000, 9001, and 9002) along with their locations in the Eldon basin. These groundwater records have been obtained from the Oklahoma Water Resources Board website (i.e., http://www.owrb.ok.gov/wd/search/search.php?type=wl).

[32] As seen in Figure 6, only the records of wells 9000 and 9002 include the period of 1995–2005, which is used in our study. Based on the records, the groundwater table has been located in about 12 ft (i.e., ~3.5 m) below the ground surface as the least depth to water during the above mentioned period, which agrees with our argument about the discussed shortness of SAC-HT.

[33] To address this issue, the upper and lower zone layers are split, and then the lower zone layers of the pixels are shifted downward throughout the basin (Figure 7). The same shift magnitude is used for all of the pixels. This introduces a new parameter to the modified model structure. The newly introduced parameter will be calibrated along with the remaining parameters in the calibrated experiment.

[34] To understand the overall performance of the modified HL-RDHM when the lower zone layers are shifted, the channel bed elevation grid (which was generated for section 4.1) along with the SAC-SMA model a priori parameters are used in the following uncalibrated experiment.

[35] To increase the potential for maximum lateral exchange between grids while ensuring full retrieval of the base flow at the basin's outlet, the primary layer bottom depth of the outlet is matched with the channel bed elevation. The same shift in magnitude is applied to the lower zone layers for the remaining pixels in the basin. This shift magnitude is only utilized for the purpose of our

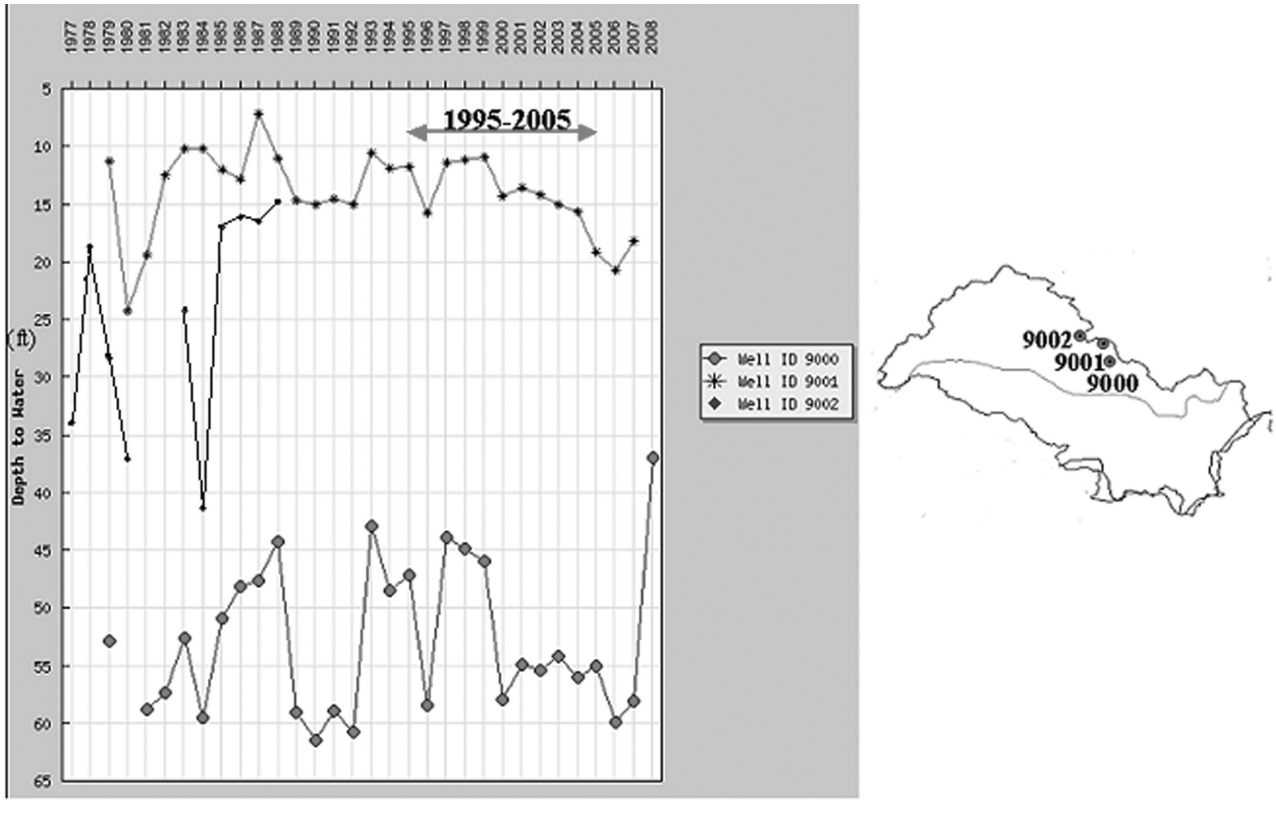

Figure 6. Groundwater level records measured at three wells (i.e., wells 9000, 9001, and 9002) along with their locations in the Eldon basin.

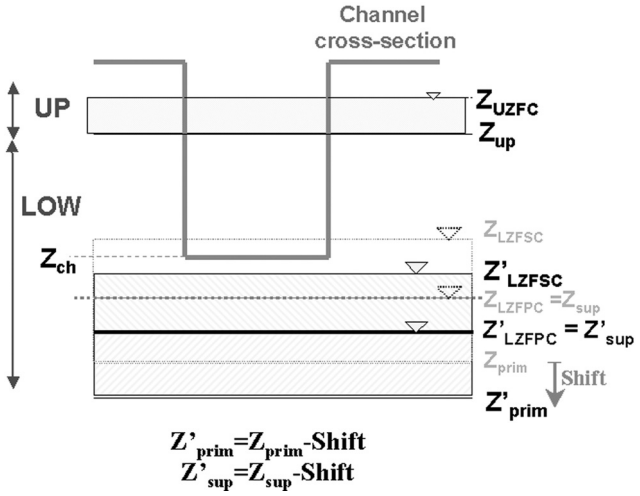

Figure 7. A schematic of the downward shifting of the lower zone layers in the physically based soil profile of a grid cell. *Z*'prim and *Z*'sup correspond to the primary and supplemental layer bottom elevations, respectively.

uncalibrated experiment. However, in the calibrated experiment, the shift magnitude will be calibrated along with the remaining model's parameters. For our test basin (i.e., the Eldon basin), a 3 m downward shifting is sufficient to match the primary layer bottom depth with the channel bed elevation at the outlet. The same 3 m downward shifting is applied to the remaining basin pixels. It is important to note that both the supplemental and primary soil layers, which are constructing elements of the lower zone, are shifted downward with the same magnitude to ensure that the supplemental layer stays presumably directly above the primary soil layer.

[36] To demonstrate the comparison between the new lower boundary elevations of supplemental and primary layers and the channel bed elevations over the test basin, the spatial plots of ($Z_{ch}-Z_{sup}$) (Figure 8a), ($Z_{ch}-Z_{prim}$) (Figure 8b), as well as the river channel network (Figure 8c), are presented for the Eldon basin. As seen in Figures 8a–8b, except for a few pixels (i.e., on the river network and close to the basin's outlet) shown in white, the remaining pixels have the lower boundary elevations of supplemental/primary layers less than the channel bed elevations and, thus have the potential to contribute to the subsurface water exchange process. Therefore, shifting the lower zone layers greatly increases the number of pixels participating in the subsurface water exchange process.

[37] The new modified HL-RDHM model with shifted lower zone layers, hereafter called the modified-shifted HL-RDHM, was run for a 10 year period (i.e., 1995–2005) over the Eldon basin using all a priori parameter grids and a 3 m shift value. As an example, Figure 9 shows the spatial and temporal variability of alpha_sup and alpha_prim generated by the modified-shifted model during the same storm event over the test basin shown in Figure 5. For both alpha_sup and alpha_prim plots, the red color represents where the alpha value is equal to one (i.e., no contribution to the water-exchange process), and the white color represents the pixels with alpha close or equal to zero (i.e., 100% contribution to water exchanges). As expected, the number of red-color pixels is greatly reduced when compared to the number of pixels given in Figures 4a and 4b. In addition, the cells representing the potential to contribute to the water exchanges shown in Figures 8a and 8b are fully contributing to the water exchanges with alpha values very close or equal to zero.

4.1.2. Sensitivity of the HL-RDHM to the Addition of the Subsurface Water Exchange Process and Shifting the Lower Zone Layers

[38] As a part of the uncalibrated experiment, an analysis is conducted to examine the level of sensitivity to the addition of the grid's subsurface water exchange process, along with shifting the lower zone layers downward by different

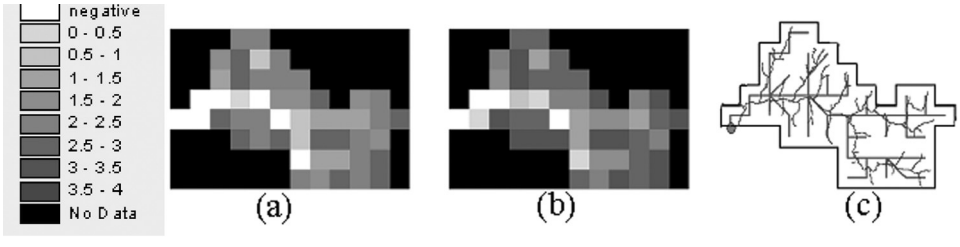

Figure 8. (a) Spatial plots of ($Z_{ch}-Z_{sup}$), (b) ($Z_{ch}-Z_{prim}$), and (c) the river channel network for the Eldon basin after shifting downward the lower zone layers.

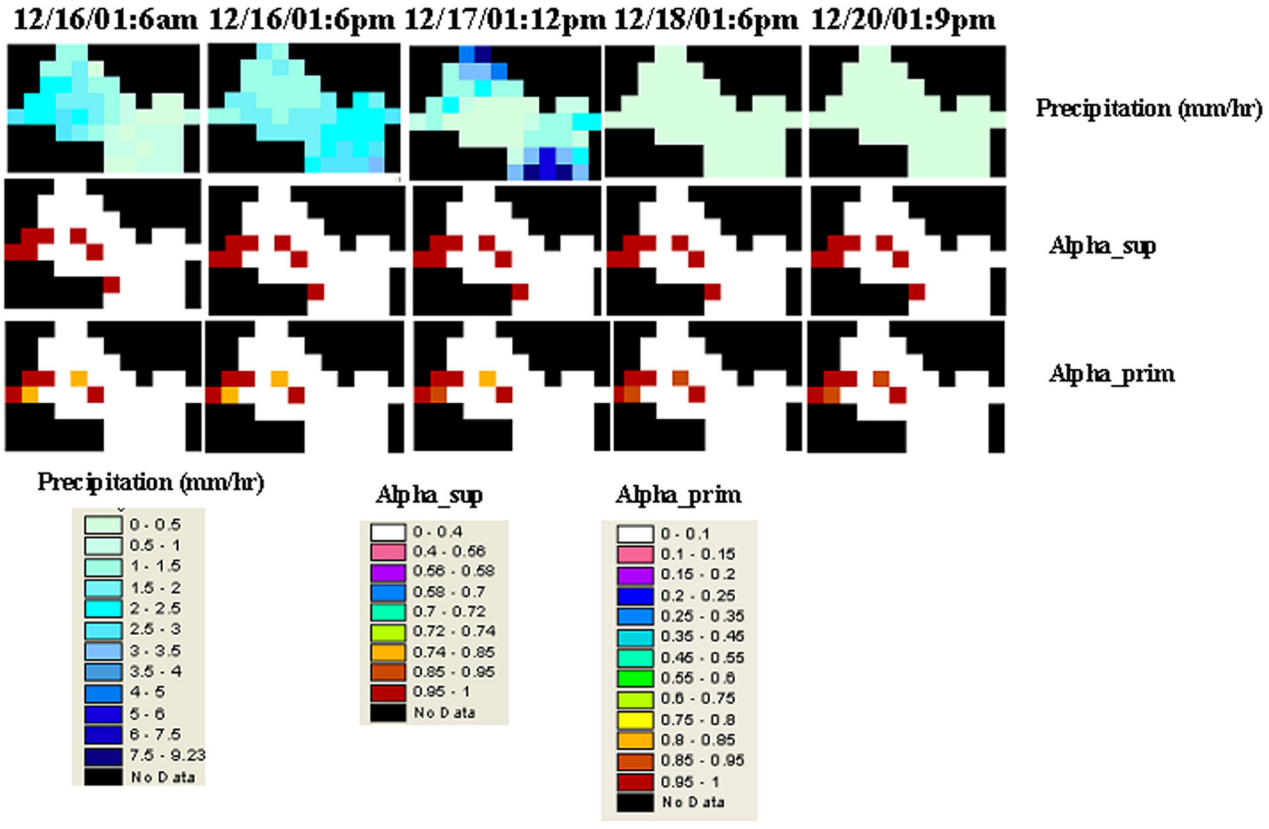

Figure 9. Spatial and temporal variability of alpha_sup and alpha_prim generated by the modified-shifted HL-RDHM during a storm event over the test basin.

shift values. Therefore, both the original and modified-shifted models are run, and the simulated discharges at several locations along the river network are compared. The stream order concept of *Strahler* [1957] is adopted to define a similar index (i.e., called pixel order) to categorize the pixels in the test basin's domain. Strahler's stream order is a numerical index to represent the complexity of the river network branching and is used to define the stream size based on a hierarchy of tributaries. Based on the connectivity order in the Eldon basin, the largest pixel-order number obtained is three. Then, from each of the pixel-order categories (i.e., 1, 2, and 3), three pixels have been chosen for the sensitivity analysis. Note that Dutch (i.e., the interior point) and Eldon (i.e., basin outlet) are in the second and third pixel-order categories, respectively. The basin outlet is chosen as one of the nine selected pixels for the sensitivity analysis. Figure 10 presents the pixel-order numbers, along with the location of the nine pixels chosen for the study. The original and modified-shifted models are run for the period of 1995–2002 to generate streamflow simulations at

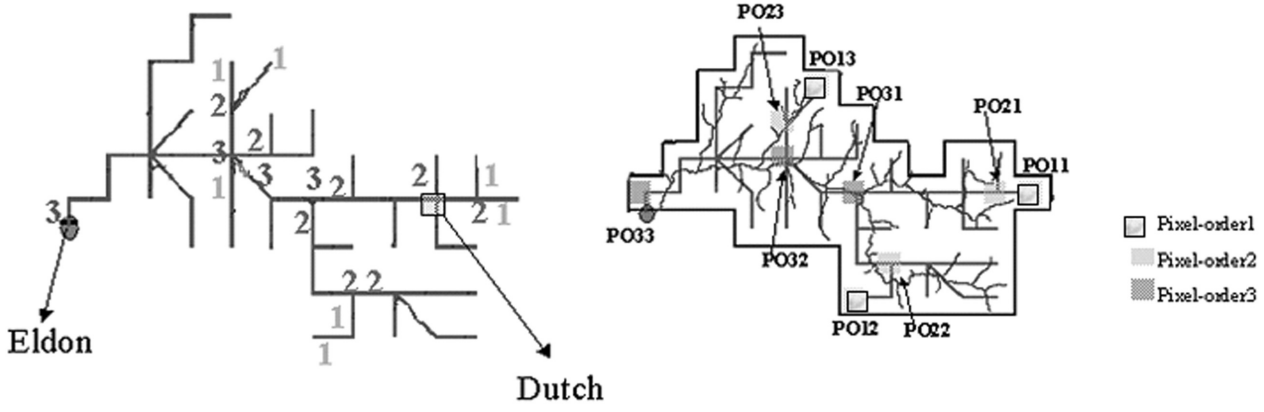

Figure 10. Pixel-order numbers along with the location of the nine pixels chosen for the study.

the nine specified pixels. To conduct the sensitivity analysis, the modified-shifted model's runs are compared to the hydrographs generated by the original HL-RDHM as a baseline. Because the original HL-RDHM's simulations are considered as the baseline for the comparison, any deviation of the modified-shifted model's simulations from the baseline is considered as the effect of the modification for subsurface exchanges plus shifting downward the lower zone layers. The deviation of the modified-shifted model's simulations from the original ones is evaluated through the use of the following statistical indices:

[39] 1. Absolute percent bias (Abs%Bias):

$$\text{Abs\%Bias} = \frac{\sum_{i=1}^{N} \left| Q_{\text{sim},i} - Q_{b,i} \right|}{\sum_{i=1}^{N} Q_{b,i}} \times 100, \tag{10}$$

where $Q_{\text{sim},i}$ represents simulated streamflow by the modified-shifted HL-RDHM and $Q_{b,i}$ represents simulated streamflow by the original model as the baseline at time step i.

[40] 2. Percent root mean square error (%RMSE):

$$\text{\%RMSE} = \frac{\sqrt{\sum_{i=1}^{N} \left(Q_{\text{sim},i} - Q_{b,i} \right)^2}}{\overline{Q_b}} \times 100, \tag{11}$$

where $\overline{Q_b}$ is the mean simulated discharge by the original HL-RDHM (i.e., baseline) over the entire time period of the analysis.

[41] Note that the larger the Abs%Bias and/or the %RMSE, the greater the difference between the modified-shifted and original models and, therefore, the bigger the impact of the modification plus shifting on the model's response.

[42] Figure 11 shows the impact of the modification for subsurface exchanges along with shifting downward the lower zone layers by different shift values (i.e., $h = 0$, -0.25, -0.5, -1, -2, and -3 m) on HL-RDHM's responses at pixels with different order categories in terms of multiyear statistics. It is important to note that the statistics at three pixels of each order category have been averaged and shown as one mean value. As seen in Figure 11, the solid bar represents the modified HL-RDHM with no shifting (i.e., $h = 0$) and is much less than the modified-shifted model results, even with a very small shift value such as $h = -0.25$ m. This implies that, in general, shifting the lower zone layers in the modified model can significantly change the responses of all pixel-order categories when compared to the original HL-RDHM simulations. In addition, both the Abs%Bias and %RMSE are generally greater at pixels of the first-order category than of the second- and third-order categories for each shift value, which in fact shows a greater impact of the modification and shifting on pixels of the first-order category than the second- and third-order categories. Moreover, by increasing the shift value at each pixel-order category, there are additions to both statistical indices. However, as can be seen in Figure 11, there is a shift value limit to the effectiveness of the modification plus shifting for each pixel-order category. As an example, a 0.5 m shift value is enough to make the pixels of the first-order category insensitive to adding more shift increments. It seems that, by shifting the lower zone layers of the pixels of the first-order category with a 0.5 m increment, their supplemental and primary layer bottom elevations become less than the channel bed elevations, resulting in the maximum contribution to the subsurface exchanges and, thus, further shifting downward cannot add to the statistics. A 2 m shift value limit also can be seen for the pixels of the second-order category.

[43] Further insight into the effect of modification for subsurface water exchange between grids plus shifting downward the lower zone layers on the HL-RDHM can be attained by looking at the result of the sensitivity analysis for three flood events with low ($Q_{\text{obs}} \sim 500$ m^3 s^{-1}), medium ($Q_{\text{obs}} \sim 1000$ m^3 s^{-1}), and high ($Q_{\text{obs}} \sim 1500$ m^3 s^{-1}) flows at the basin outlet and by computing the summary statistics of each pixel-order category, considering the original HL-RDHM runs as the baseline (Figure 12). The computed statistics, which are averaged for the three pixels of each order category, show that, in general, the modification is more effective at pixels of lower order categories, in the case of low- and medium-flow events for each shift value. However, in the high-flow event, the pixels in all three order categories seem to be affected almost equally. In

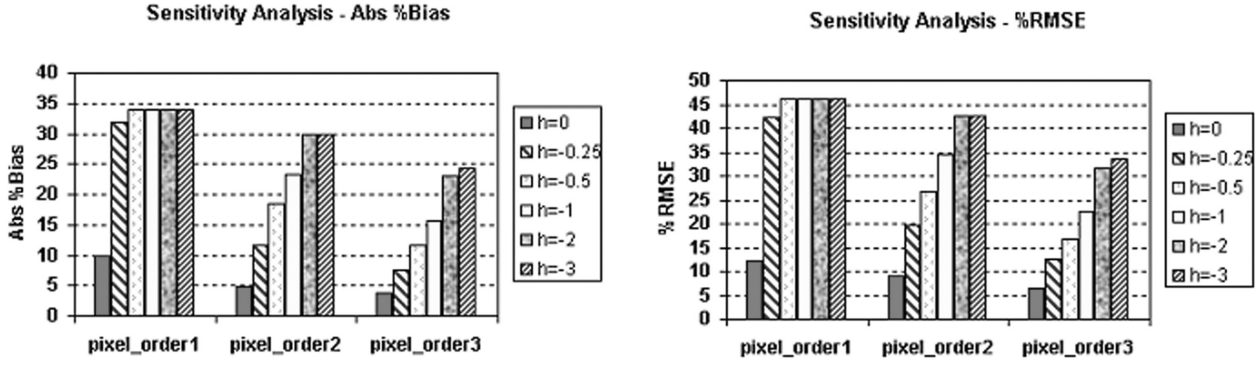

Figure 11. Impacts of the modification for subsurface water exchanges along with shifting downward the lower zone layers by different shift values (i.e., $h = 0$, -0.25, -0.5, -1, -2, and -3 m) on the HL-RDHM's responses at pixels with different order categories in terms of multiyear statistics.

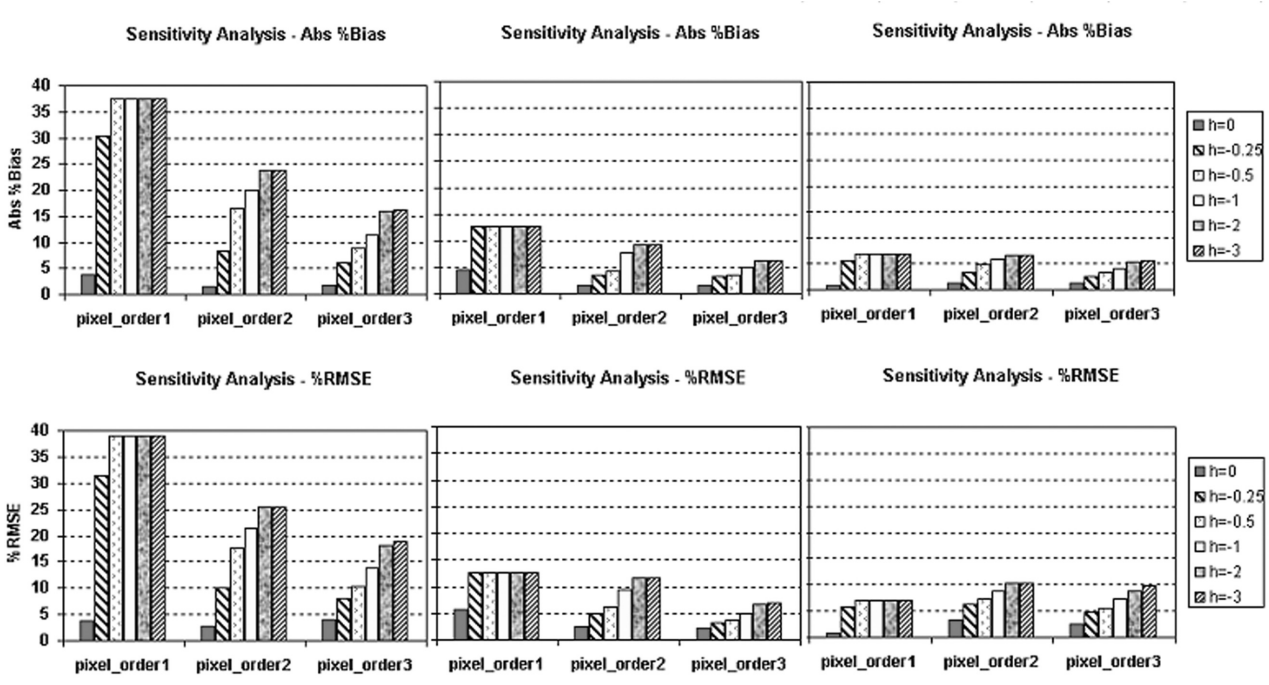

Figure 12. Impacts of the modification for subsurface water exchanges on the HL-RDHM's response at pixels with different order categories in terms of storm events. (left to right) Low-, medium-, and high-flow events.

addition, compared to the results of the modified model with no shifting (i.e., shown by solid bars), the modified-shifted HL-RDHM appears to have a greater impact on pixels from all order categories. The same shift value limits discussed in multiyear statistics can be seen in Figure 12 for first- and second-order categories.

[44] To summarize, the results shown in this section demonstrate that the addition of shifting downward the lower zone layers to the modified HL-RDHM for subsurface water exchanges significantly changes the model's responses when compared to the original model's simulations. In addition, the modified-shifted HL-RDHM has more impact on areas farther from the basin's outlet in general and in the case of low- and midflow events. However, in high-flow events, the impact of modification plus shifting the lower zone layers on all pixels of different categories is almost equal.

4.2. Calibrated Experiment

4.2.1. Model Parameters and Calibration Strategy

[45] The parameters of the modified-shifted HL-RDHM include the SAC-HT's and routing parameters, and a new parameter representing the magnitude of downward shifting in meters, equally applied to the lower zone layers of all pixels over the basin. A priori SAC-SMA model parameters developed by *Koren et al.* [2000], as well as a priori routing parameters delivered by the HL-RDHM, are basically used to account for spatial variability over a basin. Although some studies of using a priori parameters of the SAC-SMA model in lumped and distributed simulations showed that a priori parameters produced reasonably good simulations for a number of test basins [*Koren et al.*, 2000, 2006; *Duan et al.*, 2001; *Khakbaz et al.*, 2009], there are some limitations associated with their usage. For example, according to *Koren et al.* [2004], because the soil properties are only defined to a maximum depth of 2.5 m, the a priori parameters of lower zone storages are not reliable in arid regions. In addition, in the original state soil geographic (STATSGO) data, which were used to derive the a priori parameters, only representative texture values are available over large areas. Furthermore, there are some concerns about the accuracy of a priori hillslope and channel-routing parameters. Therefore, to produce improved hydrographs relative to a priori (uncalibrated) runs, the model parameters should be calibrated. The recommended strategy to calibrate the parameters of the HL-RDHM by *Koren et al.* [2004] is utilized in this study. This strategy reduces the dimension of the calibration problem, because only the parameter's scalars need to be calibrated.

4.2.2. Optimization Algorithm and Calibration Criteria

[46] The current successful automatic calibration algorithms are based primarily on global optimization. These algorithms are computationally expensive because they require a large number of function evaluations. Therefore, they are not very suitable for estimating parameters of a distributed system [*Kuzmin et al.*, 2008]. As such, a simple but computationally efficient optimization algorithm has been included in the HL-RDHM, which is called the stepwise line search (SLS) technique. According to *Kuzmin et al.* [2008], "SLS is essentially a successive minimization along coordinate directions but with a fixed step size along each coordinate and one-step propagation at a time." However, the reliability of the algorithm depends significantly

on the reliability of the a priori parameters, which are used as a starting point. Based on the comprehensive evaluation of the SLS as compared to one of the dominant global optimization algorithms in watershed model calibration (i.e., shuffled complex evolution (SCE) by *Duan et al.* [1992]), *Kuzmin et al.* [2008] reported that, while the globally optimized parameters of SCE were spread over the entire feasible parameter space when different subsets of input data were used for calibration, the posterior parameter estimates of SLS were more consistent and remained close to the a priori parameters. Furthermore, the SLS presented inferior performance than SCE in terms of reduction in both objective function on independent data set values and computational expenses. In this study the SLS algorithm is used to calibrate the parameters of the original and modified-shifted models.

[47] An objective function, which includes the contribution of several time scales, is utilized to imitate the multiscale nature of manual calibration while allowing the modeler to employ the automatic calibration algorithms. This objective function, which is called the multiscale objective function (MSOF), is defined as follows [*Kuzmin et al.*, 2008]:

$$\mathrm{MSOF} = \sqrt{\sum_{k=1}^{n} \left(\frac{\sigma_1}{\sigma_k}\right)^2 \sum_{i=1}^{m_k} (q_{o,k,i} - q_{s,k,i})^2}, \qquad (12)$$

where $q_{o,k,i}$ and $q_{s,k,i}$ are the observed and simulated discharges aggregated at time scale k, respectively, σ_k is the standard deviation of observed discharge at the kth time scale, n is the number of time scales, and m_k is the number of ordinates at time scale k. As an example, in equation (12), one can use hourly, daily, weekly, and monthly time scales corresponding to k equal to 1, 2, 3, and 4, respectively.

4.2.3. Calibrated Experiment's Results

[48] The SLS optimization algorithm and the MSOF objective function are used to calibrate both the original and modified-shifted HL-RDHM as applied to the Eldon basin. The historical record from October 1995–September 2005 was split into three periods: a warm-up period from October 1995–September 1996, a calibration period from October 1996–September 2002, and a validation period covering the remainder of the record (i.e., October 2002–September 2005). It is important to note that both models were calibrated using only the observed discharge at the basin outlet, and the observed streamflow at the interior point was disregarded during the calibration. The objective is to evaluate the ability of each model to reproduce streamflow at interior locations when observations are only available at the basin's outlet. The performances of both models are assessed through visual and statistical inspections, with the latter relying on the following:

[49] 1. Percent root mean square error (i.e., %RMSE defined in equation (11) with the exception of baseline discharge (Q_b), which needs to be replaced by observed discharge (Q_{obs})).

[50] 2. Percent bias (%Bias):

$$\%\mathrm{Bias} = \frac{\sum_{i=1}^{N} (Q_{\mathrm{sim},i} - Q_{\mathrm{obs},i})}{\sum_{i=1}^{N} Q_{\mathrm{obs},i}} \times 100. \qquad (13)$$

[51] 3. Percent absolute peak error for a given flood event ($\%E_p$):

$$\%E_p = \frac{|Q_{p,\mathrm{obs}} - Q_{p,\mathrm{sim}}|}{Q_{p,\mathrm{obs}}} \times 100, \qquad (14)$$

where $Q_{\mathrm{sim},i}$ and $Q_{\mathrm{obs},i}$ represent simulated and observed streamflow at time step i, and $Q_{p,\mathrm{sim}}$ and $Q_{p,\mathrm{obs}}$ represent simulated and observed peak flow for a given flood event, respectively. %Bias shows the total volume difference between the simulated and observed hydrographs. As such, negative (positive) biases represent model underestimation (overestimation) [*Smith et al.*, 2004].

4.2.3.1. Results at the Basin Outlet

[52] Calibration of the modified-shifted model resulted in an optimum shift value of −0.81 m. Therefore, a 0.81 m downward shifting is applied equally to the lower zone layers of all the pixels over the basin. Based on the results shown in Figure 11 and the discussion presented earlier, this shifting value is sufficient to force all of the pixels of the first-order category to participate in subsurface water exchanges. However, the 0.81 m downward shifting cannot bring the lower zone layer of the outlet (i.e., in the third-order category) beneath the channel bed at this point and, thus, the outlet still does not participate in subsurface water exchanges.

[53] To provide further insight into the performance of the original and modified models, the streamflow magnitudes at the basin outlet are classified into five equal flow intervals, which by definition represent very low, low, medium, high, and very high flows occurring at a specific point (here, basin outlet) during the calibration and validation periods. Notwithstanding the basin specificity of this classification, in general, the discharge value range between zero and the maximum observed discharge magnitude at the specified point during the study period was divided into five equal spans in order to obtain five equal flow intervals for the study. The summary statistics of the modified-shifted HL-RDHM, along with the original and modified model with no shifting (i.e., called MOD in Table 1) at the basin outlet, are presented for the above mentioned flow intervals given in Table 1 for the calibration and validation periods. The performance measures presented in Table 1 were ranked individually (superscript with parentheses) for the sake of comparison among themselves. As seen in Table 1, the modified-shifted HL-RDHM possesses an inferior performance in comparison with the original and modified models in very high-flow intervals in terms of %RMSE and in very low- and very high-flow intervals in terms of %Bias during the calibration and validation periods. However, the modified HL-RDHM with no shifting of the lower zone layers, seems to still outperform in medium- and high-flow intervals, which are indicated by improved %Bias and %RMSE during the calibration and validation periods. Overall, based on the individual ranking, the modified-shifted HL-RDHM outperforms the others in terms of %Bias during the calibration period at the basin outlet with a rank of 1.6. However, the modified HL-RDHM with no shifting possesses superior performance in terms of %RMSE during the calibration and validation periods and in terms of %Bias during the validation period (with a rank of 1.6, among others).

Table 1. Summary Statistics of the Original, Modified With No Shifting (MOD), and Modified-Shifted (MOD+SHIFT) HL-RDHM at the Basin's Outlet for the Five Equal Flow Intervals During the Calibration and Validation Periods

			Flow Intervals ($m^3 s^{-1}$)					
Calibration Period	Statistic	Model	0–310	310–620	620–929	929–1239	1239–1549	Average Rank
Eldon (outlet)	%Bias	NWS	$8.3^{(3)}$	$6.7^{(1)}$	$-9.6^{(2)}$	$-12.8^{(3)}$	$-23.5^{(3)}$	2.4
		MOD	$7^{(2)}$	$11.7^{(3)}$	$-5.7^{(1)}$	$-9.6^{(2)}$	$-20.9^{(2)}$	2
		MOD+SHIFT	$-0.4^{(1)}$	$8^{(2)}$	$-9.63^{)}$	$-4.6^{(1)}$	$-18.8^{(1)}$	1.6
	%RMSE	NWS	$99^{(1)}$	$26^{(1)}$	$25^{(2)}$	$13^{(2)}$	$24^{(3)}$	1.8
		MOD	$119^{(2)}$	$30^{(2)}$	$24^{(1)}$	$10^{(1)}$	$21^{(2)}$	1.6
		MOD+SHIFT	$158^{(3)}$	$40^{(1)}$	$28^{(3)}$	$14^{(3)}$	$19^{(1)}$	2.6

			Flow Intervals ($m^3 s^{-1}$)					
Validation Period	Statistic	Model	0–251	251–502	502–753	753–1004	1004–1255	Average Rank
Eldon (outlet)	%Bias	NWS	$12^{(3)}$	$32^{(1)}$	$-8.8^{(2)}$	$-18.6^{(2)}$	$-33.1^{(3)}$	2.2
		MOD	$10.1^{(2)}$	$39.5^{(2)}$	$-6.8^{(1)}$	$-17.5^{(1)}$	$-32^{(2)}$	1.6
		MOD+SHIFT	$0.7^{(1)}$	$45^{(3)}$	$-10^{3)}$	$-22.8^{(3)}$	$-26.2^{(1)}$	2.2
	%RMSE	NWS	$116^{(1)}$	$45^{(1)}$	$16^{(2)}$	$20^{(2)}$	$33^{(3)}$	1.8
		MOD	$133^{(2)}$	$52^{(2)}$	$15^{(1)}$	$18^{(1)}$	$32^{(2)}$	1.6
		MOD+SHIFT	$170^{(3)}$	$71^{(3)}$	$23^{(3)}$	$23^{(3)}$	$27^{(1)}$	2.6

[54] Another noteworthy observation is the phase shift in %Bias values from low flows to medium- and high-flow intervals. All three models consistently overestimate the very low and low flows but underestimate medium, high, and very high flows at the outlet during the calibration and validation periods, with the exception of the modified-shifted model in the very low-flow interval during the calibration period.

[55] Figure 13 shows two flood events, which occurred on 21 June 2000 (Figure 13, left) and 22–24 April 2004, which are two sequential events (Figure 13, right) during the calibration and validation periods, respectively. The hydrographs of the original and modified-shifted HL-RDHM from the calibrated and uncalibrated experiments for both storms, along with the observed streamflow at the basin's outlet, are shown in Figure 13. As seen in Figure 13, the calibration resulted in improved performance by both the original and modified-shifted models when compared to the uncalibrated simulations. Moreover, the addition of subsurface water exchanges and downward shifting of the lower zone layers to the HL-RDHM substantially improves the peak-flow simulations for both storm events when compared to the original model evaluated through visual and quantitative inspections, with the latter indicated by lower %Bias and $\%E_p$ for each of the given flood events with the exception of the %Bias of the given event in the validation period (Table 3).

[56] One possible reason for this result is that, in the case of high-flow events, the subsurface water exchanges increase (as a result of the gain in the base flow generation), such that the moisture deficit in the lower zone storages of the subsequent downstream pixel is satisfied. Thus, the percolation from the upper zone layer is reduced, resulting in the increase in water content of the upper zone free water

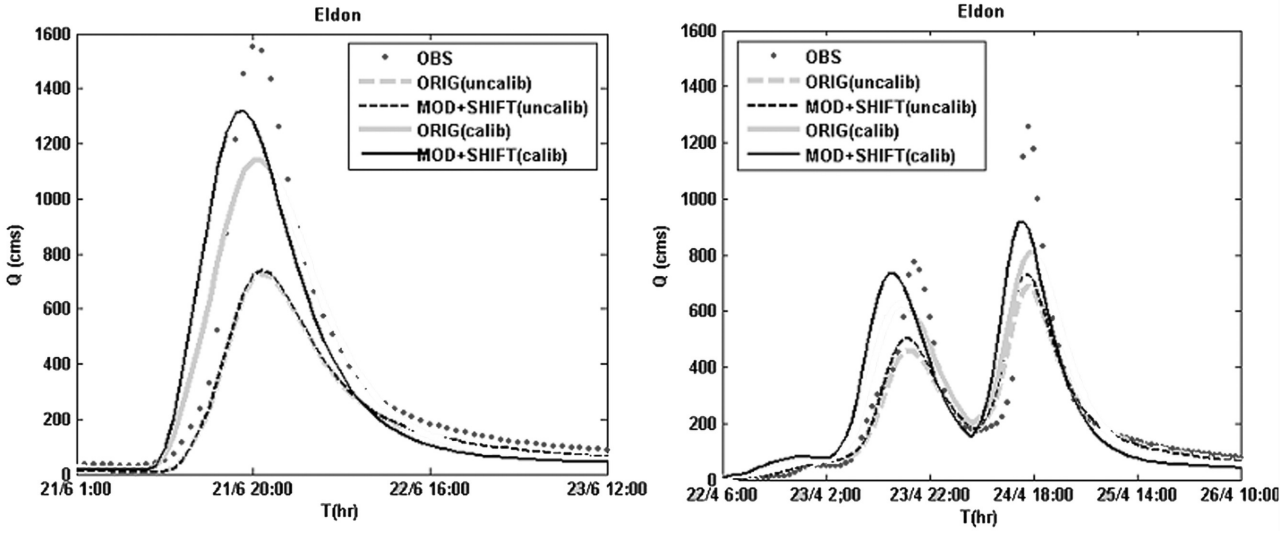

Figure 13. The uncalibrated and calibrated hydrographs generated by the original and modified-shifted models for the flood events occurring on 21 June 2000, during (left) the calibration period and 22–24 April 2004, which are two sequential events during (right) the validation period at the basin outlet.

Table 2. Summary Statistics of the Original, Modified With No Shifting (MOD), and Modified-Shifted (MOD+SHIFT) HL-RDHM at the Interior Point for the Five Equal Flow Intervals During the Calibration and Validation Periods

			Flow Intervals ($m^3 s^{-1}$)					
Calibration Period	Statistics	Model	0–112	112–225	225—337	337–449	449–561	Average Rank
Dutch (interior point)	%Bias	NWS	$12^{(3)}$	$-31.6^{(3)}$	$-30.9^{(3)}$	$-39.1^{(3)}$	$-34.9^{(3)}$	3
		MOD	$10.3^{(2)}$	$-26.1^{(2)}$	$-27.6^{(1)}$	$-34.9^{(2)}$	$-32.9^{(2)}$	1.8
		MOD+SHIFT	$-1.4^{(1)}$	$-22.7^{(1)}$	$-22.7^{(2)}$	$-29.1^{(1)}$	$-30^{(1)}$	1.2
	%RMSE	NWS	$178^{(2)}$	$62^{(3)}$	$41^{(3)}$	$39^{(3)}$	$36^{(3)}$	2.8
		MOD	$178^{(2)}$	$59^{(2)}$	$38^{(2)}$	$35^{(2)}$	$34^{(2)}$	2
		MOD+SHIFT	$175^{(1)}$	$58^{(1)}$	$36^{(1)}$	$29^{(1)}$	$32^{(1)}$	1

			Flow Intervals ($m^3 s^{-1}$)					
Validation Period	Statistics	Model	0–95	95–190	190–285	285–379	379–474	Average Rank
Dutch (interior point)	%Bias	NWS	$22.6^{(3)}$	$-16.4^{(3)}$	$-30.9^{(3)}$	$-20.9^{(3)}$	$-30.3^{(3)}$	3
		MOD	$20.7^{(2)}$	$-11.6^{(2)}$	$-30^{(2)}$	$-19.9^{(2)}$	$-29.7^{(2)}$	2
		MOD+SHIFT	$7.1^{(1)}$	$-10.1^{(1)}$	$-22.5^{(1)}$	$-16.8^{(1)}$	$-26.9^{(1)}$	1
	%RMSE	NWS	$417^{(1)}$	$42^{(3)}$	$31^{(3)}$	$22^{(3)}$	$30^{(3)}$	2.6
		MOD	$437^{(2)}$	$38^{(2)}$	$29^{(2)}$	$21^{(2)}$	$29^{(2)}$	2
		MOD+SHIFT	$450^{(3)}$	$33^{(1)}$	$23^{(1)}$	$17^{(1)}$	$27^{(1)}$	1.4

and subsequently an increase in the interflow generation. Overall this results in an increase in the magnitude of the peak flow generated by the modified-shifted model as compared to the original model's hydrograph. However, in the case of low-flow events as can be seen from the falling limb of the hydrographs in Figure 13, the subsurface water coming from the upstream pixel is not able to fully satisfy the moisture deficit of the lower zone storages (as a result of general reduction in the base flow magnitudes). Thus, percolation from the upper zone storages remains almost unchanged. Therefore, comparing to the high-flow conditions, the subsurface exchanges not only do not increase the interflow but also reduce the base flow contribution to the total generated discharge. Overall, in low-flow conditions, the subsurface water exchanges between grids result in decreasing the flow magnitudes as compared to the original HL-RDHM hydrographs.

4.2.3.2. Results at the Interior Point

[57] The summary statistics of the original, modified with no shifting, and modified-shifted HL-RDHM at the interior point (i.e., the Dutch basin) are presented for the above-described five equal flow intervals presented in Table 2 for the calibration and validation periods. Except for the %Bias at the medium-flow interval during the calibration period and the %RMSE in the very low-flow interval during the validation period, the modified-shifted HL-RDHM outperforms the other two models, which is indicated by improved %Bias and %RMSE during the calibration and validation periods for all flow intervals.

[58] Figure 14 shows the same two flood events displayed in Figure 13 with the hydrographs of the original and modified-shifted HL-RDHM from the calibrated and uncalibrated experiments, along with the observed streamflow at the Dutch basin. As seen in Figure 14, calibration using the observed discharge at the outlet resulted in improved interior point simulations of both the original and modified-shifted models when compared to the uncalibrated simulations. Moreover, for both storm events, the modified-shifted HL-RDHM improves the peak flow simulations when compared to the original HL-RDHM model, both visually and quantitatively (Table 3).

[59] Based on the results of the calibrated experiment, it can be perceived that shifting downward the lower zone layers in the modified HL-RDHM could obviously improve the streamflow simulations at the interior point compared to the original HL-RDHM model. However, the modified-shifted model does not provide much improvement in the basin's outlet compared to the modified HL-RDHM with no shifting, with the exception of the gain in accuracy in very high peak flow simulations. Even though modification of the original HL-RDHM for the subsurface water exchange process enhances the model's ability in streamflow simulation, this result is limited to this test basin and needs to be evaluated in other basins as well.

Table 3. Summary Statistics of the Original and Modified-Shifted HL-RDHM at the Outlet and the Interior Point for the Two Flood Events Occurring on 21 June 1997 and 22–24 April 2004 During the Calibration and Validation Periods, Respectively

Location	Statistics	Model	Calibration Period	Validation Period
Eldon (Outlet)	%Bias	NWS	−15.6	4.86
		MOD+SHIFT	−11.0	7.9
	$\%E_p$	NWS	40.0	35.5
		MOD+SHIFT	27.2	26.6
Dutch (Interior Point)	%Bias	NWS	−28.1	−1.2
		MOD+SHIFT	−27.9	−0.6
	$\%E_p$	NWS	54.4	30.3
		MOD+SHIFT	48.5	26.9

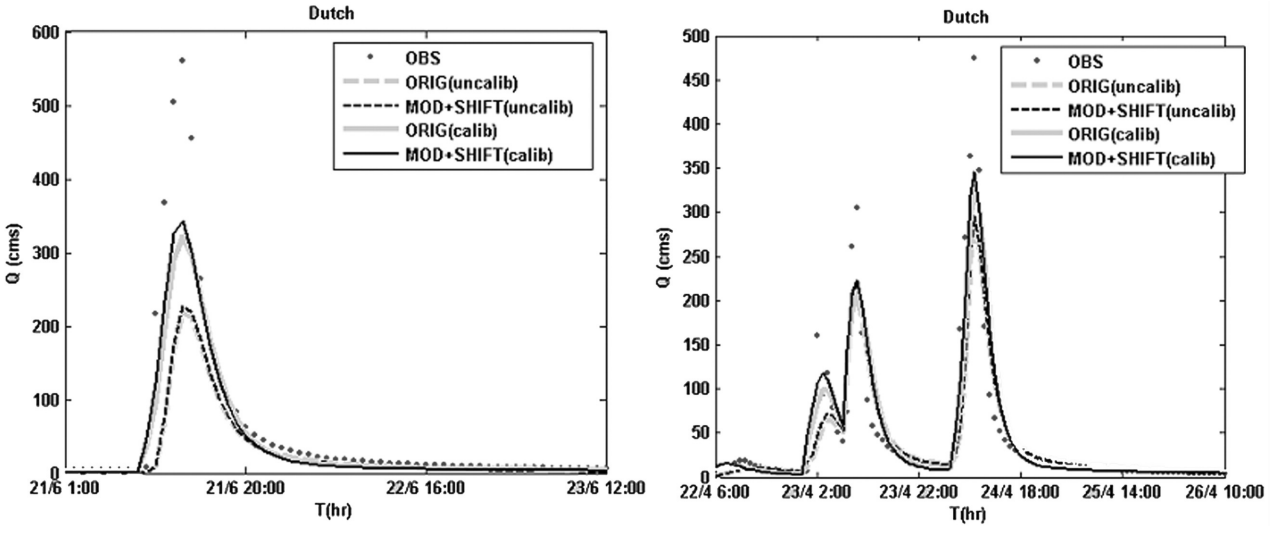

Figure 14. The uncalibrated and calibrated hydrographs generated by the original and modified-shifted models for the flood events occurring on 21 June 2000, during (left) the calibration period and 22 and 24 April 2004, which are two sequential events during (right) the validation period at the interior point.

5. Summary and Conclusions

[60] The NWS distributed hydrologic model (i.e., HL-RDHM) was modified for subsurface water exchanges between grids. The subsurface water exchange process was established by partitioning the slow response components released from the lower layer storages into two parts: the first part involved the grid's conceptual channel, while the second was added to the lower layer storages of the downstream pixel. By using the a priori parameters, the original and modified models were applied in Baron Fork at Eldon, Oklahoma, as the study test basin. Ten years of grid-based multisensor (NEXRAD + gauge) precipitation data were used to investigate the effects of the modification on model performance. The results of the uncalibrated experiment showed that there are few pixels in the basin, which had the potential to contribute to the supplemental water exchange process. In addition, most of the pixels on the channel network did not participate in the primary water exchanges. The main reason was that the SAC-HT locates the physical layers in relatively shallow depths, which limited participation of several cells over the basin's domain in the subsurface water exchange process.

[61] Realizing the deficiency of the SAC-HT to locate the lower zone layers in sufficient depths (i.e., 2 m), a complementary study was conducted to test the feasibility of further improvement in the modified model by shifting downward the lower zone layers of all pixels equally over the basin. The sensitivity analysis revealed that a greater number of pixels contributed to the subsurface water exchanges when the lower zone layers were shifted downward. The original and modified-shifted HL-RDHM models were then calibrated using a simple local search algorithm (i.e., called SLS) and a multiscale objective function (i.e., MSOF) at the basin's outlet, without utilizing the interior point information. The results of the calibration experiment showed that modification of the model for the subsurface water exchange process with no shifting of the lower zone layers led to improvement in peak flow simulations at the basin's outlet. In addition, the calibrated modified-shifted HL-RDHM could markedly improve the streamflow simulations at the interior point compared to the original HL-RDHM model. However, the modified-shifted model does not provide much improvement in the basin's outlet compared to the modified HL-RDHM with no shifting of the lower zone layers, except with the gain in accuracy of simulations in very high peak flow events.

[62] Even though the modified-shifted HL-RDHM generally presented better performance than the original model, especially for the interior point, this result is limited to this test basin and needs to be validated in other basins as well. Therefore, the application of the modified HL-RDHM on basins with different climatology than the test basin used here is one of the future extensions to this study.

[63] It is worth mentioning that modification of the HL-RDHM for subsurface water exchanges between grids adds more complexity to the model structure and, therefore, can introduce more uncertainties into the results. There are several possible sources of uncertainty, which can be listed as follows:

[64] 1. The assumption that the hydraulic gradient of the subsurface flow is equal to the ground-surface slope.

[65] 2. Uncertainty in the channel bed elevation estimations.

[66] 3. The methodology to locate the lower zone layers in the modified-shifted model.

[67] The above mentioned uncertainties may have contributed to the resulting discrepancies in the modified model's performance. Analyses of these uncertainties and exploring the new ways to address these issues are the subjects of future studies.

[68] Under operational conditions, an important consideration in the modification of a model structure is the ease of transition from the original model to the modified structure. The proposed approach, which does not introduce more

than one parameter to the model structure, provides exactly the type of smooth transition required to gain the support of forecasters. The modification did not dramatically alter the model's structure, allowing its application with the use of recently available parametric and input data.

[69] In summary, the focus of the study was mainly on the improvement of a hydrologic model applicable to flood predictions at a wide range of river basins. While SW–GW interaction parameterization was developed specifically for the NWS distributed hydrologic model, it may be applicable to a range of watershed models, which do not have explicit channel groundwater interfaces.

[70] Finally, the improvements in model performance by modification of subsurface water exchanges between grids, while not very significant at the basin's outlet, were clear in terms of producing better simulations at the interior points which remarks the main conclusion of the study. This is an important lesson, which may contribute to the current debate about lumped versus distributed models, especially in the case of interior point simulations.

[71] **Acknowledgments.** Partial support for this research was provided by the National Oceanic and Atmospheric Administration (NOAA) and National Weather Service (NWS) Office of Hydrologic Development (OHD) through the Research Foundation of City University of NY (CUNY) (grant 49,100-01A). The authors would like to thank Dan Braithwaite for his assistance in data processing. We also would like to thank Praveen Kumar and the anonymous reviewers for their valuable comments.

References

Beasley, R. S. (1976), Contribution of subsurface flow from the upper slopes of forested watersheds to channel flow, *Soil Sci. Soc. Am. J.*, *40*, 955–957.

Beeson, P. C., S. N. Martens, and D. D. Breshears (2001), Simulating overland flow following wildfire: Mapping vulnerability to landscape disturbance, *Hydrol. Processes*, *15*, 2917–2930.

Beven, K. J. (1989), Interflow, in *Unsaturated Flow in Hydrologic Modeling: Theory and Practice*, edited by H. J. Morel-Seytoux, pp. 191–219, Kluwer, Dordrecht.

Beven, K. J., and M. J. Kirkby (1979), A physically based variable contributing area model of basin hydrology, *Hydrol. Sci. Bull.*, *24*(1), 43–69.

Burnash, R. J. C., R. L. Ferral, and R. A. McGuire (1973), Joint Federal-State River Forecast Center, A generalized streamflow simulation system; Conceptual modeling for digital computers, p. 204, U.S. Dept. of Commerce National Weather Service and State of California Dept. of Water Resources, Sacramento, Calif.

Croley, T. E., and C. He (2006), Watershed surface and subsurface spatial intraflows model, *J. Hydrol. Eng.*, *11*(1), doi:10.1061/(ASCE)1084-0699(2006)11:1(12).

Dincer, T., B. R. Payne, T. Florkowski, J. Martinec, and E. Tongiorgi (1970), Snowmelt runoff from measurements of tritium and oxygen-18, *Water Resour. Res.*, *6*, 110–124, doi:10.1029/WR006i001p00110.

Dingman, S. L. (1994), *Physical Hydrology*, Macmillan, New York.

Duan, Q. Y., S. Sorooshian, and V. Gupta (1992), Effective and efficient global optimization for conceptual rainfall–runoff models, *Water Resour. Res.*, *28*(4), 1015–1031, doi:10.1029/91WR02985.

Duan, Q., J. Schaake, and V. Koren (2001), A priori estimation of land surface model parameters, in *Land Surface Hydrology, Meteorology, and Climate: Observations and Modeling Water Science and Application 3*, edited by V. Lakshmi et al., pp. 77–94, AGU, Washington, D. C.

Freeze, R. A. (1974), Streamflow generation, *Rev. Geophys. Space Phys.*, *12*, 627–647, doi:10.1029/RG012i004p00627.

Furman, A. (2008), Modeling coupled surface-subsurface flow processes: A review, *Vadose Zone J.*, *7*, 741–756.

Greene, D. R., and M. D. Hudlow (1982), Hydrometeorologic grid mapping procedures, AWRA International Symposium on Hydrometeorology, Denver, Colo.

Gulden, L. E., E. Rosero, Z. L. Yang, M. Rodell, C. S. Jackson, G. Y. Niu, P. J. F. Yeh, and J. Famiglietti (2007), Improving land-surface model hydrology: Is an explicit aquifer model better than a deeper soil profile?, *Geophys. Res. Lett.*, *34*, L09402, doi:10.1029/2007GL029804.

Khakbaz, B., B. Imam, K. Hsu, and S. Sorooshian (2009), From lumped to distributed via semi-distributed: Calibration strategies for semi-distributed hydrologic models, *J. Hydrol.*, doi:10.1016/j.jhydrol.2009.02.021.

Kim, C. P., G. D. Salvucci, and D. Entekhabi (1999), Groundwater–surface water interaction and the climatic spatial patterns of hillslope hydrological response, *Hydrol. Earth Syst. Sci.*, *3*, 375–384.

Kollet, S. J., and R. M. Maxwell (2006), Integrated surface–groundwater flow modeling: A free-surface overland flow boundary condition in a parallel groundwater flow model, *Adv. Water Resour.*, *29*, 945–958.

Kong, J., P. Xin, Z. Y. Song, and L. Li. (2010), A new model for coupling surface and subsurface water flows: With an application to a lagoon, *J. Hydrol.*, *390*, 116–120.

Koren, V. (2006), Parameterization of frozen ground effects: Sensitivity to soil properties, in *Predictions in Ungauged Basins: Promise and Progress*, edited by M. Sivapalan, T. Wagener, S. Uhlenbrook, E. Zehe, V. Lakshmi, X. Liang, Y. Tachikawa, and P. Kumar, pp. 125–133, IAHS Press, Wallingford, U. K.

Koren, V. I., M. Smith, D. Wang, and Z. Zhang (2000), Use of soil property data in the derivation of conceptual rainfall-runoff model parameters, in *15th Conference on Hydrology*, pp. 103–106, American Meteorological Society, Long Beach, CA (preprints).

Koren, V., M. Smith, and Q. Duan (2003), Use of a priori parameter estimates in the derivation of spatially consistent parameter sets of rainfall-runoff models, in *Calibration of Watershed Models: Water Science and Application Series*, vol. 6, edited by Q. Duan, H. Gupta, S. Sorooshian, A. Rousseau, and R. Turcotte, AGU, Washington, D. C.

Koren, V., S. Reed, M. Smith, Z. Zhang, and D.-J. Seo (2004), Hydrology Laboratory Research Modeling System (HL-RMS) of the U.S. National Weather Service, *J. Hydrol.*, *291*, 297–318.

Koren, V., F. Moreda, S. Reed, M. Smith, and Z. Zhang (2006), Evaluation of a grid-based distributed hydrological model over a large area, in *Predictions in Ungauged Basins: Promise and Progress*, edited by M. Sivapalan, T. Wagener, S. Uhlenbrook, E. Zehe, V. Lakshmi, X. Liang, Y. Tachikawa, and P. Kumar, IAHS Publication, *303*, pp. 47–56, IAHS Press, Wallingford, U. K.

Koren, V., F. Moreda, and M. Smith (2008), Use of soil moisture observations to improve parameter consistency in watershed calibration, *Phys. Chem. Earth, Parts A/B/C*, *33*(17–18), 1068–1080.

Kuzmin, V., D. J. Seo, and V. Koren (2008), Fast and efficient optimization of hydrologic model parameters using a priori estimates and stepwise line search, *J. Hydrol.*, *353*(1–2), 109–128.

Leavesley, G. H., R. W. Lichty, B. M. Troutman, and L. G. Saindon (1983), Precipitation-runoff modeling system: User's manual, *U.S. Geological Survey Water-Resources Investigations, 83-4238*, 207 p.

Martinec, J., U. Siegenthaler, H. Oeschger, and E. Tongiorgi (1974), New insights into the run-off mechanism by environmental isotopes, in *Isotope Techniques in Groundwater Hydrology*, pp. 129–149, IAEA, Vienna, Austria.

Maxwell, R. M., and N. L. Miller (2005), Development of a coupled land surface and groundwater model, *J. Hydrometeorol.*, *6*, 233–247.

Moreda, F., V. Koren, Z. Y. Zhang, S. Reed, and M. Smith (2006), Parameterization of distributed hydrological models: Learning from the experiences of lumped modeling, *J. Hydrol.*, *320*(1–2), Special Issue SI, 218–237.

Mosley, M. P. (1979), Streamflow generation in a forested watershed, New Zealand, *Water Resour. Res.*, *15*(4), 795–806, doi:10.1029/WR015i004p00795.

Panday, S., and P. S. Huyakorn (2004), A fully coupled physically based spatially-distributed model for evaluating surface/subsurface flow, *Adv. Water Resour.*, *27*, 361–382.

Pinder, G. F., and J. F. Jones (1969), Determination of the ground-water component of peak discharge from the chemistry of total runoff, *Water Resour. Res.*, *1*(2), 438–445, doi:10.1029/WR005i002p00438.

Pokhrel, P., H. V. Gupta, and T. Wagener (2008), A spatial regularization approach to parameter estimation for a distributed watershed model, *Water Resour. Res.*, *44*, W12419, doi:10.1029/2007WR006615.

Qu, Y., and C. J. Duffy (2007), A semi-discrete finite volume formulation for multiprocess watershed simulation, *Water Resour. Res.*, *43*, W08419, doi:10.1029/2006WR005752.

Reed, S., V. Koren, Z. Zhang, M. Smith, and D.-J. Seo (2002), Distributed modeling for improved NWS river forecasts, in *Proceedings of the*

Second Federal Interagency Hydrologic Modeling Conference, Las Vegas, NV.

Reed, S., V. Koren, M. Smith, Z. Zhang, F. Moreda, and D. J. Seo (2004), Overall distributed model intercomparison project results, *J. Hydrol.*, *298*(1–4), 27–60.

Reed, S., J. Schaake, and Z. Y. Zhang (2007), A distributed hydrologic model and threshold frequency-based method for flash flood forecasting at ungauged locations, *J. Hydrol.*, *337*(3–4), 402–420.

Singh, V. P., and D. A. Woolhiser (2002), Mathematical modeling of watershed hydrology, *J. Hydrol. Eng.*, *7*(4), 270–292.

Sklash, M. G., and R. N. Farvolden (1979), The role of groundwater in storm runoff, *J. Hydrol.*, *43*, 45–65.

Smith, M. B., D. Seo, V. I. Koren, S. M. Reed, Z. Zhang, Q. Duan, F. Moreda, and S. Cong (2004), The Distributed Model Intercomparison Project (DMIP): Motivation and experiment design, *J. Hydrol.*, *298*, 4–26.

Sophocleous, M. (2002), Interactions between groundwater and surface water: The state of the science, *Hydrogeol. J.*, *10*, 52–67.

Strahler, A. N. (1957), Quantitative analysis of watershed geomorphology, *Am. Geophys. Union Trans.*, *38*, 913–920.

Tang, Y., P. Reed, K. Van Werkhoven, and T. Wagener (2007), Advancing the identification and evaluation of distributed rainfall-runoff models using global sensitivity analysis, *Water Resour. Res.*, *43*, W06415. doi:10.1029/2006WR005813.

Tóth, J. (1962), A theory of groundwater motion in small drainage basins in central Alberta, Canada, *J. Geophys. Res.*, *67*(11), 4375–4387, doi:10.1029/JZ067i011p04375.

VanderKwaak, J. E., and K. Loague (2001), Hydrologic-response simulations for the R-5 catchment with a comprehensive physics-based model, *Water Resour. Res.*, *37*, 999–1013, doi:10.1029/2000WR900272.

Van Werkhoven, K., T. Wagener, P. Reed, and Y. Tang (2008), Rainfall characteristics define the value of streamflow observations for distributed watershed model identification, *Geophys. Res. Lett.*, *35*, L11403. doi:10.1029/2008GL034162.

Wagener, T., K. Van Werkhoven, P. Reed, and Y. Tang (2009), Multi-objective sensitivity analysis of the information content in streamflow observations for distributed watershed modeling, *Water Resour. Res.*, *45*, W02501, doi:10.1029/2008WR007347.

Woolhiser, D. A. (1996), Search for physically based runoff model—A hydrologic el Dorado?, *J. Hydrol. Eng.*, *122*(3), 122–129.

Yilmaz, K. K., H. V. Gupta, and T. Wagener (2008), A process-based diagnostic approach to model evaluation: Application to the NWS distributed hydrologic model, *Water Resour. Res.*, *44*, W09417, doi:10.1029/2007WR006716.

Z. Cui, V. I. Koren, P. Restrepo, and M. B. Smith, Hydrology Laboratory, Office of Hydrologic Development, WOHD-12 NOAA/National Weather Service, 1325 East-West Hwy., Silver Spring, MD 20910, USA.

B. Imam, B. Khakbaz, and S. Sorooshian, Center for Hydrometeorology and Remote Sensing, Department of Civil and Environmental Engineering, University of California, E4130 Engineering Gateway, Irvine, CA 92697, USA. (behkhakbaz@yahoo.com)